Rossby waves on the Sun as revealed by solar 'hills'

J. R. Kuhn*, J. D. Armstrong*, R. I. Bush† & P. Scherrer†

** Institute for Astronomy, University of Hawaii, 2680 Woodlawn Drive, Honolulu, Hawaii 96822, USA*
† Stanford University, HEPL 4085, Stanford, California 94305, USA

It is a long-standing puzzle that the Sun's photosphere—its visible surface—rotates differentially, with the equatorial regions rotating faster than the poles. It has been suggested[1] that waves analogous to terrestrial Rossby waves, and known as r-mode oscillations, could explain the Sun's differential rotation: Rossby waves are seen[2] in the oceans as large-scale (hundreds of kilometres) variations of sea-surface height (5-cm-high waves), which propagate slowly either east or west (they could take tens of years to cross the Pacific Ocean). Calculations show that the solar r-mode oscillations have properties that should be strongly constrained by differential rotation[3]. Here we report the detection of 100-m-high 'hills' in the photosphere, spaced uniformly over the Sun's surface with a spacing of $(8.7 \pm 0.6) \times 10^4$ km. If convection under the photosphere is organized by the r-modes, the observed corrugated photosphere is a probable surface manifestation of these solar oscillations.

The notion that global Rossby, or inertial, waves could exist within a rotating star was first described in calculations by Papaloizou and Pringle[4]. They named these toroidal oscillations r-modes, after Rossby waves. Unlike the intermediate period g-modes[5], whose properties are determined by buoyancy restoring forces, the nearly incompressible r-modes are subject to Coriolis forces and have periods which are near the rotation period. They have not been convincingly observed, but detailed calculations[3,6,7] imply that these modes are a potent probe of the largest structures in the solar convection zone, because they sample both the solar rotation and the large-scale convection timescales. With sufficient amplitude, r-modes will even affect a star's convection and differential rotation flows as suggested in ref. 1.

The Michelson Doppler Imager (MDI) on board the Solar and Heliospheric Observatory (SOHO) was designed primarily for Doppler observations, although it has produced unique astrometric data because of its accurate pointing and imaging capability from above the Earth's atmosphere. Recently, MDI improved on other attempts to measure the static solar limb shape by achieving an uncertainty of less than one milliarcsec (ref. 8) in the solar quadrupole and hexadecapole shape. Figure 1 illustrates the astrometric sensitivity of the technique—here the solar shape distortion produced by global p-modes has been detected. These modes (which

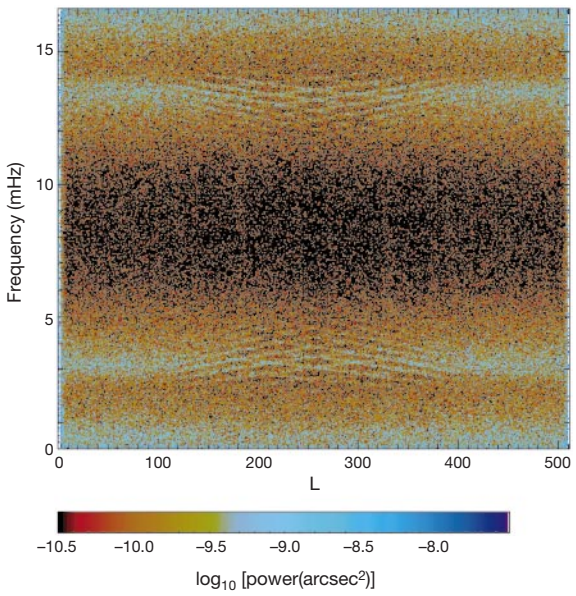

Figure 1 The two-dimensional power spectrum of the limb displacement. This was derived from an 8-h period of 1-min cadence data obtained in position angle bins 0.7° wide. The horizontal axis corresponds to the angular frequency (L, in units of waves per cycle) while the vertical axis plots the temporal frequency. We note that a measurement at angular frequency k tends to sample spherical harmonic modes of angular and azimuthal order equal to $k(l = m = k)$. The image colourscale indicates the logarithm of the derived limb displacement power in units of arcsec^2. This figure shows the complete spectrum, including Nyquist aliasing about the central temporal and spatial frequencies. The p-mode ridge structure near frequencies of 3 mHz is clearly observed here in the changing solar limb shape.

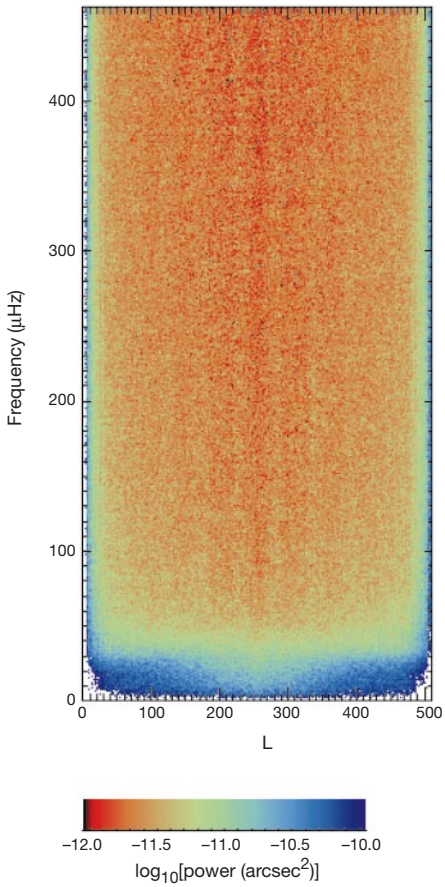

Figure 2 The two-dimensional, low-frequency, power spectrum of the MDI limb timeseries. Over a period of 26 months, a 6-pixel-wide annulus which includes the solar limb was generated every 12 min (ref. 9). These data were analysed as described in ref. 7 to reveal the limb position and brightness in 512 position angle bins covering the solar limb, and with 98,304 temporal samples at a cadence of 12 min. Gaps from telemetry problems and instrument mode changes corrupted ~3% of this timeseries. Measurements obtained after the SOHO disruption on 25 June 1998 and after the spacecraft reacquired the Sun on 16 September 1998 were also not included here because of a higher noise background caused by frequent spacecraft and experiment operating mode changes. The horizontal axis describes the angular frequency as obtained from the discrete transform with respect to the limb position angle. Slowly varying instrumental noise was minimized by removing a 180° wide boxcar average from each limb data record. An 8.3-d boxcar temporal average was also removed to yield a record of the residual temporal fluctuations in the solar limb over a 2.2-yr period. The two-dimensional Fourier transform yields the limb displacement power spectral density in units of arcsec^2 per frequency bin, which is displayed here on a logarithmic colourscale.

are of intermediate spherical harmonic degree, and which have 5-min periods) have radial amplitudes of about 15 cm s^{-1} so that one oscillation mode produces a limb displacement amplitude of about 10 microarcsec. This is consistent with the amplitude of the ridge structure displayed in Fig. 1 as it was measured from 8 hours of 1-min cadence MDI solar limb data.

Measurements of longer-period oscillations are possible using the nearly continuous MDI dataset obtained between 19 April 1996 and 24 June 1998 (ref. 10). Analysis of the MDI limb timeseries (Fig. 2) clearly shows excess low frequency power on all spatial scales below 25 μHz. The corresponding displacement velocity amplitude (Fig. 3) shows an obvious power excess near 20 μHz with a root-mean-square velocity amplitude of about 0.3 mm s^{-1}. This is not likely to be caused by low radial and angular order solar g-modes because such modes more efficiently penetrate the convection zone to reach the photosphere at higher frequencies corresponding to periods of one to a few hours (ref. 5).

The temporal signature of a photospheric structure (for example, a standing wave pattern) as it traverses the limb due to solar rotation can be detected in the temporal power spectrum of the limb displacement, computed as a function of position angle (or solar latitude). The apparent sawtooth-shaped power enhancement in Fig. 4 is consistent with a co-rotating photospheric modulation having a latitude-independent transverse scale of $(8.7 \pm 0.6) \times 10^4$ km. As expected for a solar (rather than an instrumental) phenomenon, the power distribution near the poles is noticeably smeared by the 7° inclination of the solar rotation axis from the normal direction to the ecliptic plane. We also analysed data from approximately one month when the MDI was rotated several degrees from its nominal roll angle. Data obtained during this period confirms that this signal is not associated with the MDI instrument, because the 'sawtooth' power distribution, calculated as in Fig. 4, rotated in apparent position angle by an amount in agreement with the new MDI roll angle.

This regular structure of 100-m-high photospheric 'hills', uniformly spaced over the surface of the Sun with a characteristic separation of approximately 90,000 km, is most plausibly explained as the co-rotating photospheric signature of long period r-modes. It is not surprising that these modes have been invisible from the ground, as long-period oscillations are more readily detected from astrometric (shape) measurements from space than from even the most sensitive ground-based Doppler observations. At low frequencies, solar Doppler data are dominated by incoherent velocity noise from the convection zone. At low temporal frequencies, even a small velocity amplitude oscillation may be extracted from the convective noise in limb shape measurements because the limb displacement amplitude grows linearly with oscillation period (for a constant velocity amplitude), while the convection noise contributes only incoherently.

We now consider if this signal could be produced by the solar supergranulation[11]. With a transverse scale of 30,000 km, the timescale for limb perturbations due to these features would be 4 h, or about one-third of the period of the observed 20 μHz power excess. We could propose that only the largest supergranule elements are detected at the limb because of foreshortening and projection effects. Then, depending on the statistical distribution of supergranules, we might find only one-in-two or one-in-three of them to be visible at the limb. With the assumption that supergranulation is a random convection process we expect the timeseries of limb perturbations to be random, but with a mean time between limb perturbations of, say, 11 h. This stochastic timeseries (called a "random telegraph signal"[12]) has a well-known power spectrum, $P(\omega)$, in the form of a lorentzian function, $P(\omega) = P_0/[1 + (\omega/\omega_0)^2]$, where P_0 and ω_0 are parameters that characterize the amplitude and mean frequency of the random telegraph signal. Thus, the existence of a mean timescale (11 h in this case) leads to a spectrum which is monotonic, and which shows a $1/\omega^2$ decline beyond the characteristic frequency. Only if there is long-range coherence in the

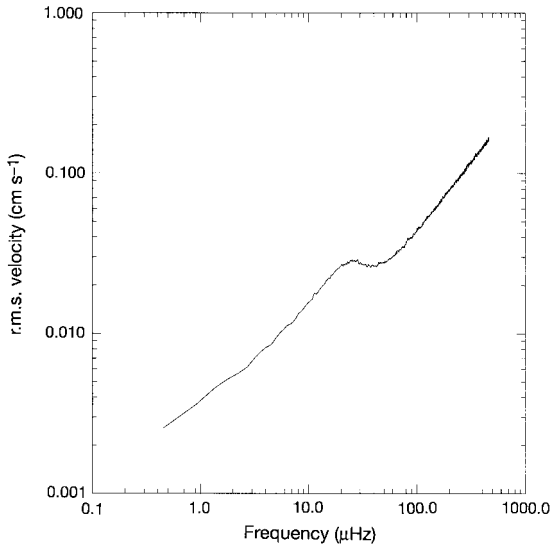

Figure 3 Root-mean-square limb shape velocity amplitude plotted against frequency. The average displacement power between angular frequencies of L and 256 has been converted to an r.m.s. velocity by scaling the amplitude by the temporal frequency. This is plotted on a logarithmic scale to reveal the mean effective velocity background from 800 d of astrometric observations. The excess power appears here as a bump at a frequency near 20 μHz with a total r.m.s. amplitude of 0.03 cm s^{-1}.

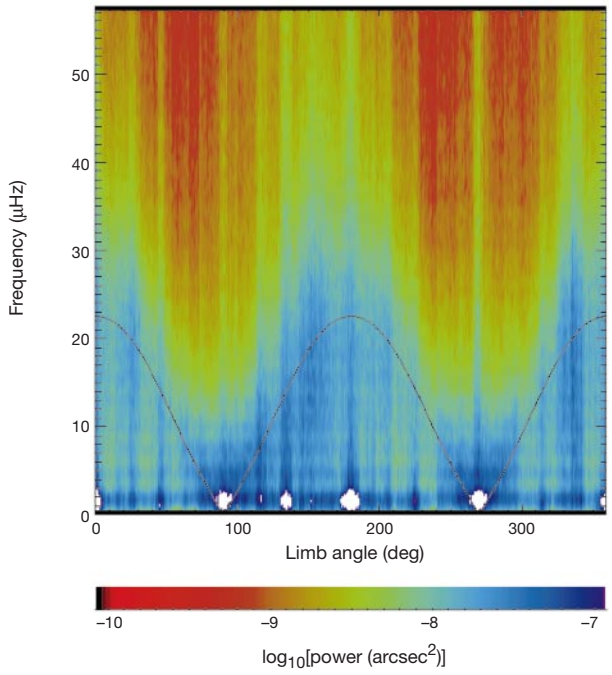

Figure 4 The power distribution plotted here shows the average power per temporal frequency bin versus position angle. The colourscale describes the average power in units of $arcsec^2$ per bin on a logarithmic intensity scale. The limb displacement was computed from the residual of a 256-bin running mean of each limb position record. Temporal residuals were then evaluated from the difference between this computed limb position and an 8.3-d running mean of the timeseries (duration, 7.1×10^7 s). Position angle 0 corresponds to the west limb with increasing angles approaching the solar north pole. The power spectrum has been smoothed with an 88-point running boxcar average before plotting. The solid line shows the expected frequency of vertical photospheric modulation, with a transverse scale of 8.75×10^4 km, which is rotating at the photospheric differential rotation rate.

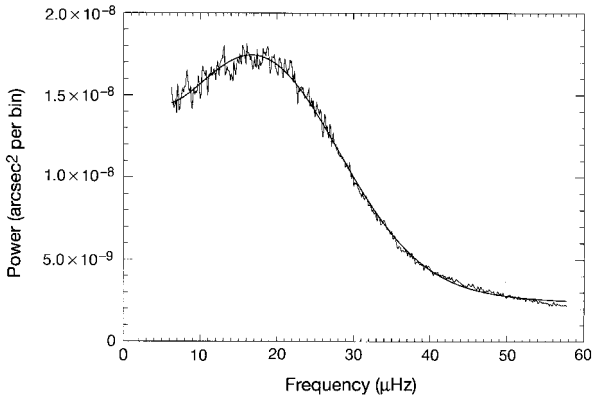

Figure 5 The mean power spectrum averaged over solar latitude. This was computed by assuming that the limb power spectra are due to a photospheric displacement pattern, rotating across the limb at various velocities corresponding to the local latitudinal rotation speed. The mean spectrum is obtained by first stretching the frequency scale of each latitudinal spectrum to match the equatorial spectrum (by linear interpolation onto the new frequency domain), and then averaging these on the common frequency domain. A simple shift of each spectrum by a frequency equal to the sawtooth variation with latitude (from Fig. 4) also matches the broad power excess at each latitude to the equatorial rate, yielding a mean spectrum which is essentially the same as the scaled frequency result displayed here. The solid line shows a least-squares fit to a gaussian and a power-law background distribution. The resulting centre frequency is 18 μHz.

timeseries (over many characteristic timescales) will the power spectrum yield a peak at the average temporal frequency. Thus, a test of the stochastic or supergranule hypothesis requires looking for a lorentzian form to the low-frequency spectrum.

The spectrum from a single latitude bin is too noisy to distinguish a monotonic excess power signal (a lorentzian) from the generally increasing displacement noise power towards lower frequencies. Combining spectra from a range of latitude bins improves the signal-to-noise ratio. We find a gaussian peak in the mean spectrum (Fig. 5) with a centre frequency of 18 μHz. The existence of a spectral peak suggests that at least a portion of the low-frequency power is not caused by supergranules. Although the spectrum also contains a displacement 'background' signal which increases to lower frequencies, the peak signal (corresponding to a 15-h period) is best described as a low-Q oscillator. It has long-range order and is not a stochastic 'random telegraph'. A standing wave is a natural mechanism for producing such a lattice of solar 'hills'. Wolff[13,14] previously suggested that a large-scale photospheric nodal pattern generated by phase-locked r-modes would evolve over timescales of a few days—a result in qualitative agreement with the low-Q oscillator we see here in the mean limb displacement power spectrum. If r-modes are driven by the largest scales of convection, we should also expect a characteristic length scale of the order of the depth of the convection zone: that is, 2×10^5 km. The transverse scale we observe is half this, but is plausibly consistent.

The magnitude of the vertical displacement is also energetically reasonable. If subphotospheric convection is spatially organized by Rossby modes, then even velocities of 100 m s^{-1} (a small fraction of measured photospheric convective velocities) are energetic enough to lift up the overlying photosphere by the observed 100-m vertical height. Although it remains to be seen from detailed model calculations exactly how global solar r-modes could be excited, the existence of a corrugated photosphere with long-range order is good evidence for these oscillations. □

Received 16 December 1999; accepted 16 March 2000.

1. Plaskett, H. H. The polar rotation of the Sun. *Mon. Not. R. Astron. Soc.* **131,** 407–433 (1966).
2. Chelton, D. B. & Schlax, M. G. Global observations of oceanic Rossby waves. *Science* **272,** 234–238 (1996).
3. Wolff, C. L. Linear r-mode oscillations in a differentially rotating star. *Astrophys. J.* **502,** 961–967 (1998).
4. Papaloizou, J. & Pringle, J. E. Non-radial oscillations of rotating stars and their relevance to the short-period oscillations of cataclysmic variables. *Mon. Not. R. Astron. Soc.* **182,** 423–442 (1978).
5. Kumar, P., Quataert, E. & Bahcall, J. Observational searches for solar g-modes: some theoretical considerations. *Astrophys. J.* **458,** 83–L85 (1996).
6. Provost, J., Berthomeiu, G. & Rocca, A. Low frequency oscillations of a slowly rotating star—quasi toroidal modes. *Astron. Astrophys.* **94,** 126–133 (1981).
7. Wolff, C. L. & Blizard, J. B. Properties of r-modes in the Sun. *Sol. Phys.* **105,** 1–15 (1986).
8. Kuhn, J. R., Bush, R., Scheick, X. & Scherrer, P. The Sun's shape and brightness. *Nature* **392,** 155–157 (1998).
9. Lazrek, M. *et al.* First results on p-modes from GOLF experiment. *Sol. Phys.* **175**, 227–246 (1997).
10. Scherrer, P. H. *et al.* The solar oscillations investigation—Michelson Doppler Imager. *Sol. Phys.* **162,** 129–188 (1995).
11. Schrijver, C. J., Hagenaar, H. R. & Title, A. M. On the patterns of the solar granulation and supergranulation. *Astrophys. J.* **475,** 328–337 (1997).
12. Rice, S. O. Mathematical analysis of random noise. *Bell Syst. Tech. J.* **23,** 1–162 (1944).
13. Wolff, C. L. Distinctive patterns on the surface of slowly rotating stars whose oscillations are non-linearly coupled. *Astrophys. J.* **193,** 721–727 (1974).
14. Wolff, C. Oscillation convection coupling: cause of supergranulation. *Astrophys. J.* **443,** 423–433 (1995).

Acknowledgements

We thank J. Saba, C. DeForest and J. Covington for assistance in operating the MDI instrument during these observations. We are particularly grateful to R. Bogart and to X. Scheick for their help with the limb software analysis.

Correspondence and requests for materials should be addressed to J.R.K. (e-mail: jkuhn@solar.stanford.edn).

Acceleration of quantum decay processes by frequent observations

A. G. Kofman & G. Kurizki

Department of Chemical Physics, The Weizmann Institute of Science, Rehovot 76100, Israel

In theory, the decay of any unstable quantum state can be inhibited by sufficiently frequent measurements—the quantum Zeno effect[1–10]. Although this prediction has been tested only for transitions between two coupled, essentially stable states[5–8], the quantum Zeno effect is thought to be a general feature of quantum mechanics, applicable to radioactive[3] or radiative decay processes[6,9]. This generality arises from the assumption that, in principle, successive observations can be made at time intervals too short for the system to change appreciably[1–4]. Here we show not only that the quantum Zeno effect is fundamentally unattainable in radiative or radioactive decay (because the required measurement rates would cause the system to disintegrate), but also that these processes may be accelerated by frequent measurements. We find that the modification of the decay process is determined by the energy spread incurred by the measurements (as a result of the time–energy uncertainty relation), and the distribution of states to which the decaying state is coupled. Whereas the inhibitory quantum Zeno effect may be feasible in a limited class of systems, the opposite effect—accelerated decay—appears to be much more ubiquitous.

We recall the common argument leading to the quantum Zeno effect (QZE)[3,4]. If a system ruled by hamiltonian $\hat{H}$ is in state $|e\rangle$ at $t = 0$, the probability to find the system there at $t > 0$ is:

$$\rho_{ee}(t) = \left| \left\langle e \left| \exp\left(-\frac{i}{\hbar}\hat{H}t \right) \right| e \right\rangle \right|^2 \qquad (1)$$